Constitutive Relation for Ambient-Temperature Creep in Hexagonal Close-Packed Metals

Tetsuya Matsunaga[1,*1], Tatsuya Kameyama[2,*2], Kohei Takahashi[3,*3] and Eiichi Sato[4]

[1]*Department of Space and Astronautical Science, School of Physical Sciences, The Graduate University for Advanced Studies, Sagamihara 229-8510, Japan*
[2]*Department of Materials Engineering, School of Engineering, The University of Tokyo, Tokyo 113-8656, Japan*
[3]*Department of Aerospace Engineering, School of System Design, Tokyo Metropolitan University, Tokyo 191-0065, Japan*
[4]*The Institute of Space and Astronautical Science, Japan Aerospace Exploration Agency, Sagamihara 229-8510, Japan*

This paper reports creep tests on three kinds of polycrystalline hexagonal close-packed metals, i.e. commercially pure titanium, pure magnesium, and pure zinc, in the vicinity of ambient temperature even below their 0.2% proof stresses. These materials showed significant steady state creep rates around $10^{-9}\,\text{s}^{-1}$ and had stress exponents of about 3.0. Arrhenius plots in the vicinity of ambient temperature indicate extremely low apparent activation energies, Q, of about 20 kJ/mol, which is at least one-fourth of the Q of dislocation-core diffusion. Ambient-temperature creep also has a grain-size effect with an exponent of 1.0. These parameters indicate that ambient-temperature creep is a new creep deformation mechanism in h.c.p. materials. [doi:10.2320/matertrans.M2009223]

1. Introduction

Titanium (Ti) and its alloys are useful materials for aerospace and transport industries. Particularly, Ti-6Al-4V alloys are used as main structural materials because of their high specific strength, high corrosion resistance, and amenability to superplastic blow forming. The Institute of Space and Astronautical Science, Japan Aerospace Exploration Agency (ISAS/JAXA) developed Ti-6Al-4V alloy fuel tanks, which have been used for scientific satellites for 25 years.[1] The 'HAYABUSA' spacecraft launched in 2003 also possesses tanks of this type. When one of these tanks was pressurized in a proof test,[2] creep behavior was observed at ambient temperature even below a 0.2% proof stress. Although small creep strain in a fuel tank might be permissible, using Ti-6Al-4V alloy as a fastener, i.e. a bolt or a nut, will bring about stress relaxation, possibly leading a component to breakdown and destruction. Therefore, it is important for the industry to elucidate the behavior of ambient-temperature creep.

Ambient-temperature creep was observed about one half century ago in pure Ti.[3–5] Since that time, several studies of this phenomenon have been carried out using Ti alloys. Several Ti alloys[6] were investigated in the 1960s and 70s such as Ti-5Al-2.5Sn alloy[7,8] and Ti-6Al-4V alloy.[7,9–11] Later, Mills' group[12–17] intensively studied this phenomenon using Ti-6Al and Ti-6Al-2Sn-4Zr-2Mo. Among these experimental studies restricted to Ti alloys, the present authors found recently that all hexagonal close-packed (h.c.p.) metals and alloys show creep behavior at ambient temperature below their 0.2% proof stresses,[18] but no cubic metals or

alloys show creep behavior under the same condition. The former group included commercially pure Ti (CP-Ti), pure magnesium (Mg), pure zinc (Zn), Ti-6Al-4V, Zircaloy, and AZ31, and the latter group included pure iron, 5052Al, and Ti-15V-3Cr-3Sn-3Al. Additionally, we introduced a new region into the Ashby-type deformation mechanism map of annealed CP-Ti,[19] the ambient-temperature creep region.[20]

The present study summarizes parameters of ambient-temperature creep in typical pure h.c.p. metals, i.e. CP-Ti, Mg, and Zn, through wide-temperature-ranged creep tests. Using pure metals avoids the influence of substitutional solute atoms, whose importance to ambient-temperature creep was established by Neeraj *et al.*[13] However, because deformation of Ti is influenced strongly by oxygen (O) content, three Ti sheets with well characterized O contents were also examined. The intragranular deformation mechanism will be discussed in a forthcoming paper.[21]

2. Experimental Procedure

This work used rolled sheets of CP-Ti (JIS grade 1) designated as CP-Ti 1A as well as pure Mg and pure Zn. Other rolled sheets of CP-Ti (JIS grade 1) designated as CP-Ti 1B, and CP-Ti (JIS grade 2) designated as CP-Ti 2, were also examined. The measured chemical compositions, pre-treatments and c/a ratios of these sheets are listed in Table 1. Temperature-dependent Young's moduli calculated from Ashby's textbook[19] for CP-Ti, Mg, and Zn are listed in Table 1. The grain sizes, d, as measured by the linear intercept method were 75, 75, 17, 120 and 100 μm for CP-Ti 1A, CP-Ti 1B, CP-Ti 2, Mg, and Zn, respectively. Optical micrographs of these materials are shown in Fig. 1. Coarse-grained Zn samples with grain sizes of 210 and 1500 μm were produced by annealing at 483 K and 573 K for 24 h, respectively.

Tensile tests were performed to evaluate 0.2% proof stresses ($\sigma_{0.2}$) at ambient temperature with a constant cross-head speed corresponding to an initial strain rate of

Table 1 Measured chemical compositions, pre-treatments, crystallographic c/a ratios, Temperature-dependent Young's moduli of the five examined specimens.

Samples	Chemical composition[*1] (mass%)	Pre-treatment	c/a	$E(T)^{*2}$/GPa[19]
CP-Ti 1A (grade 1)	Ti-0.03Fe-0.04O-0.002H-0.01C-0.01N	973 K air cooling	1.589	$1.15 \times 10^5(1 + (-1.2(T - 300)/1933))$
CP-Ti 1B (grade 1)	Ti-0.03Fe-0.06O-0.002H-0.01C-0.01N	973 K air cooling	1.589	$1.15 \times 10^5(1 + (-1.2(T - 300)/1933))$
CP-Ti 2 (grade 2)	Ti-0.06Fe-0.09O-0.0002H-0.01C-0.01N	973 K air cooling	1.589	$1.15 \times 10^5(1 + (-1.2(T - 300)/1933))$
Mg	99.95Mg-0.003Al-0.003Si-0.008Mn-0.005Zn	573 K hot rolling	1.624	$4.26 \times 10^4(1 + (-0.49(T - 300)/924))$
Zn	99.995Zn	hot rolling	1.856	$1.23 \times 10^5(1 + (-0.5(T - 300)/693))$

[*1]Oxygen contents in CP-Ti sheets were measured by graphite furnace atomic absorption spectrometry.
[*2]Poisson's rations, i.e. 0.318 (CP-Ti), 0.289 (Mg), and 0.244 (Zn),[22] were used to translate G into E.
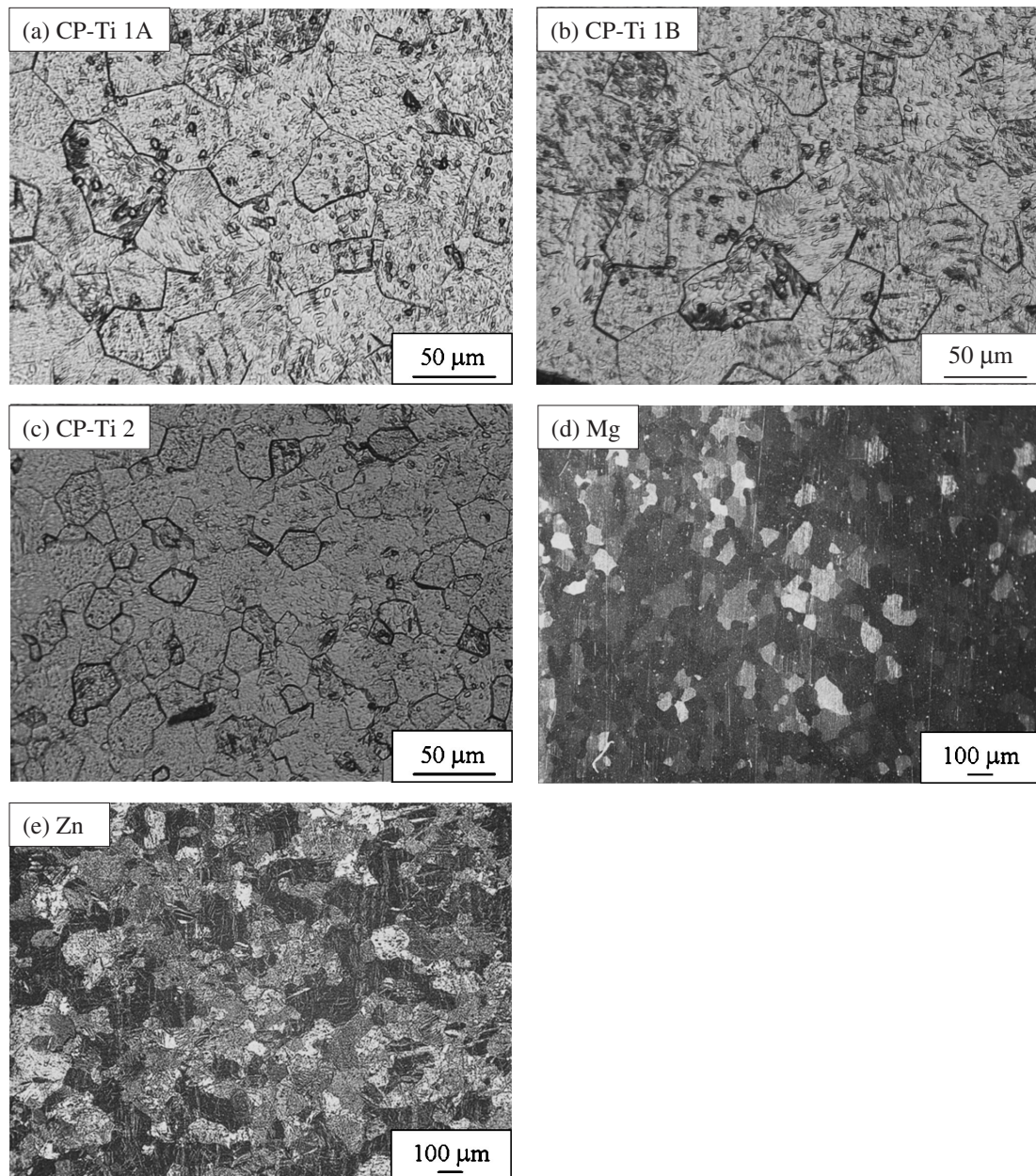
Fig. 1 Optical micrographs of (a) CP-Ti 1A, (b) CP-Ti 1B, (c) CP-Ti 2, (d) Mg and (e) Zn with $d = 100 \, \mu m$.
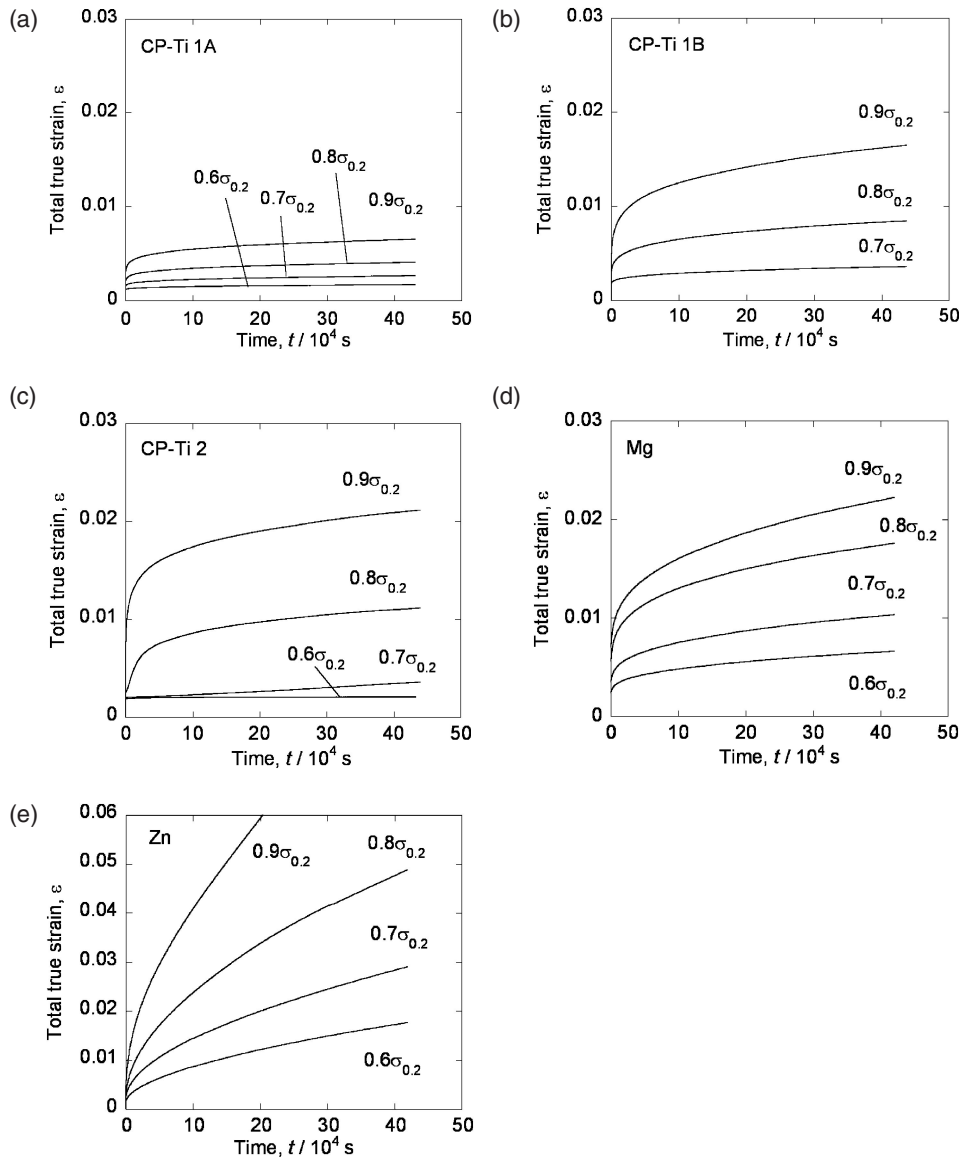
Fig. 2 Creep curves of (a) CP-Ti 1A, (b) CP-Ti 1B, (c) CP-Ti 2, (d) Mg and (e) Zn with $d = 100\,\mu$m at ambient temperature under loads of 0.6–0.9$\sigma_{0.2}$, where $\sigma_{0.2}$ at ambient temperature is 176, 220, 280, 61 and 40 MPa for each material, respectively.

$1 \times 10^{-3}\,\text{s}^{-1}$ using an Instron-type machine. Creep tests were performed in tension using a dead-load creep frame at temperatures from 203 K to 873 K and with loads of 0.6–0.9$\sigma_{0.2}$, where the $\sigma_{0.2}$ were obtained at ambient temperature. Tensile and creep specimens were prepared using a wire electrical discharge machine with the loading direction corresponding to the rolling direction. Tensile and creep strains were measured using strain gauges with a resolution of 3×10^{-6} mounted directly on the specimen surface. By reducing the creep of the strain gauge itself, a strain rate of $3 \times 10^{-10}\,\text{s}^{-1}$ was measured directly.[18] For creep tests at temperatures higher than 473 K, strain was measured using an optical displacement camera with an accuracy of 10^{-4}.

3. Experimental Results

The 0.2% proof stresses ($\sigma_{0.2}$) at ambient temperature were 176, 220, 280, 61 and 40 MPa for CP-Ti 1A, CP-Ti 1B, CP-Ti 2, Mg and Zn with $d = 100\,\mu$m, respectively. Figure 2

displays creep curves of the tested materials at ambient temperature with a load of 0.6–0.9$\sigma_{0.2}$, which show significant creep behavior. These creep curves were fitted by the logarithmic creep equation[23] to evaluate steady state creep rates:

$$\varepsilon = \varepsilon_0 + \varepsilon_\text{p} \ln(1 + \beta_\text{p}t) + \dot{\varepsilon}_\text{s}t, \qquad (1)$$

where ε is the true strain, ε_0 is the instantaneous strain, ε_p and β_p are parameters characterizing the primary creep region, $\dot{\varepsilon}_\text{s}$ is the extrapolated steady state creep rate, and t is the elapsed time. This equation was formulated using eq. (2) on the basis of dislocation kinetics by Li[24] and Akulov:[25]

$$\varepsilon = \varepsilon_0 + \frac{\dot{\varepsilon}_\text{s}}{k_1} \ln\left\{1 + \frac{\dot{\varepsilon}_\text{i} - \dot{\varepsilon}_\text{s}}{\dot{\varepsilon}_\text{s}}(1 - e^{-k_1t})\right\} + \dot{\varepsilon}_\text{s}t, \qquad (2)$$

where $\dot{\varepsilon}_\text{i}$ is the initial creep rate and k_1 is the dislocation multiplication rate constant. At low temperatures, because $\dot{\varepsilon}_\text{i}/\dot{\varepsilon}_\text{s} \gg 0$ and $k_1t \ll 1$, eq. (2) becomes eq. (1), as proposed by Garofalo.[23] In this study we used a fitting eq. (1) because
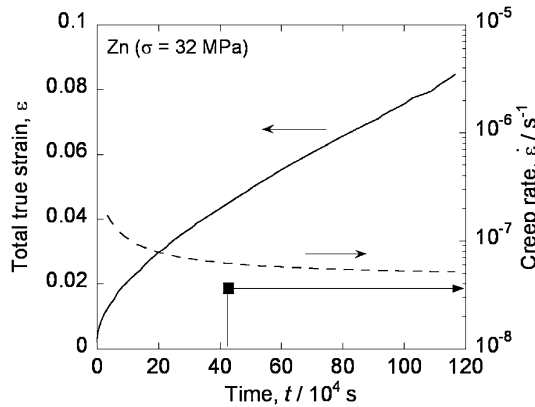
Fig. 3 Creep strain and strain rate curves of Zn with $d = 100\,\mu m$ at 298 K under 32 MPa ($0.8\sigma_{0.2}$). The solid square is the extrapolated steady state creep rate, $\dot{\varepsilon}_s$, determined by eq. (1) using creep data up to 4.3×10^5 s. This value is almost identical to the creep rate (broken line) at 1.1×10^6 s, where creep behavior seems to be at steady state.

Fig. 4 Double logarithmic plots of the modulus-compensated applied stress and the extrapolated steady state creep rate for all specimens at ambient temperature. The stress exponents are about 3.0 for CP-Ti 1A, Mg and Zn with $d = 100\,\mu m$, whereas they are 5.5 for CP-Ti 1B and 6.0 for CP-Ti 2.

our earlier study revealed that the power-law creep equation does not fit the experimental creep curve well but the logarithmic creep equation does.[20]

Figure 3 shows total true strain and strain rate curves for Zn with $d = 100\,\mu m$ under a stress of 32 MPa ($= 0.8\sigma_{0.2}$). The extrapolated steady state creep rate using the creep data up to 4.3×10^5 s is shown as a solid square in Fig. 3. This extrapolated steady state creep rate of $3.7 \times 10^{-8}\,s^{-1}$ is almost identical to the creep rate of $5.1 \times 10^{-8}\,s^{-1}$ obtained directly from the creep curve at 1.1×10^6 s. The creep behavior seems to be in a steady state after 4.0×10^5 s. In this study, extrapolated steady state creep rates using creep data up to 4.3×10^5 s were used for the entire analysis.

Figure 4 shows a double logarithmic plot of σ/E and $\dot{\varepsilon}_s$ for all five specimens at 298 K. The n values are about 3.0 for CP-Ti 1A, Mg and Zn with $d = 100\,\mu m$, 5.5 for CP-Ti 1B, and 6.0 for CP-Ti 2. For CP-Ti, the n value increased from 3.0 to 6.0 as the impurity content increased from 0.04 mass% O to 0.09 mass% O, which implies that the n value is strongly influenced by O content. In addition, the samples with higher O content (CP-Ti 2) show inverse transition behavior because of the Cottrell effect (Fig. 2(c) $0.6\sigma_{0.2}$ and $0.7\sigma_{0.2}$). These results revealed that CP-Ti 1A clearly belongs to the pure-metal group along with Mg and Zn. In further analyses, CP-Ti 1A was treated as a pure metal without the solute strengthening effect.

For the pure-metal group of CP-Ti 1A, Mg and Zn with $d = 100\,\mu m$, Fig. 5 shows a double logarithmic plot of modulus compensated applied stress, σ/E, and $\dot{\varepsilon}_s$ at temperatures from 203 K to 873 K. These plots are divided into two regions. The values of the stress exponents, n, are about 3.0 for the three metals in the lower temperature region around ambient temperature. In regions with temperatures higher than 723 K, 343 K and 343 K for the three metals, respectively, the n values range between 4.0 and 5.0. These n values are similar to that of the low-temperature dislocation creep region with dislocation-core diffusion.

Arrhenius plots are shown in Fig. 6 for CP-Ti 1A at $\sigma/E = 0.001$, Mg at $\sigma/E = 0.0008$, and Zn with $d = 100\,\mu m$ at $\sigma/E = 0.0002$ from 203 K to 873 K, where T is temperature and Q is the apparent activation energy. These plots are
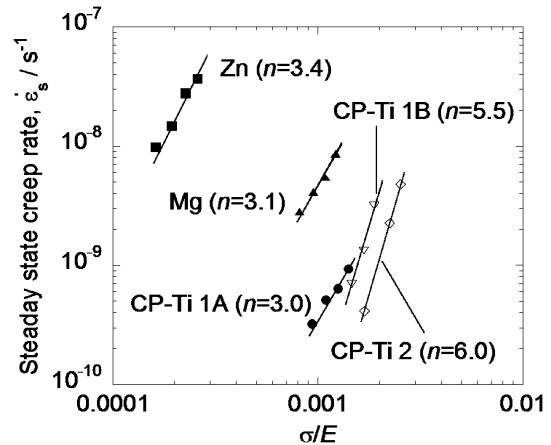
divided into two regions for Mg and Zn. The higher-temperature regions, at temperatures higher than 330 K and 320 K for Mg and Zn, respectively, have larger apparent activation energies of 64 and 79 kJ/mol. These regions correspond to the low-temperature dislocation creep regions, where creep proceeds at a rate controlled by the recovery rate of dislocations through dislocation-core diffusion, which has an activation energy about 0.65 times[19] that of lattice diffusion, 135 and 92 kJ/mol[19] for Mg and Zn, respectively. For CP-Ti 1A, the data from 373 K to 573 K were omitted because the creep rates at these temperatures were almost negligible due to the strain aging effect.[26] Therefore, the Q value in the low-temperature dislocation creep region could not be determined. The higher-temperature region above 573 K has a Q value of 150 kJ/mol and corresponds to the high-temperature dislocation creep region controlled by lattice diffusion with $Q = 150$ kJ/mol.[19]

Figure 6 shows also an ambient-temperature creep region, which shows extremely low Q values of about 20 kJ/mol. This region does not appear in the deformation mechanism maps produced by Frost and Ashby,[19] and was first drawn into a map by Tanaka et al. for CP-Ti.[20] Figure 6 reveals that this ambient-temperature creep region extends down to at least 203 K for the three tested metals. Even for Zn, room temperature, 0.43 of the melting temperature, belongs to the ambient-temperature creep region.

Figure 7 shows the grain-size dependence of ambient-temperature creep of Zn under $0.8\sigma_{0.2}$, which corresponds to 32, 19 and 4.8 MPa for the specimen with $d = 100$, 210, and 1500 μm, respectively. Creep strain decreases with increasing grain size; the specimen with $d = 1500\,\mu m$ shows brittle fracture without creep deformation.

For Zn with $d = 100$ and 210 μm, a double logarithmic plot of σ/E and $\dot{\varepsilon}_s$ is shown in the right part of Fig. 8. This shows that the $\dot{\varepsilon}_s$ of coarse-grained specimens decreases by one order of magnitude compared with the fine-grained specimens. The grain-size exponent, p, was determined as 1.0 for Zn from left part of Fig. 8, a double logarithmic plot of $\mathbf{b}/d$ and $\dot{\varepsilon}_s$ at $\sigma/E = 0.004$, where $\mathbf{b}$ is the Burgers vector.
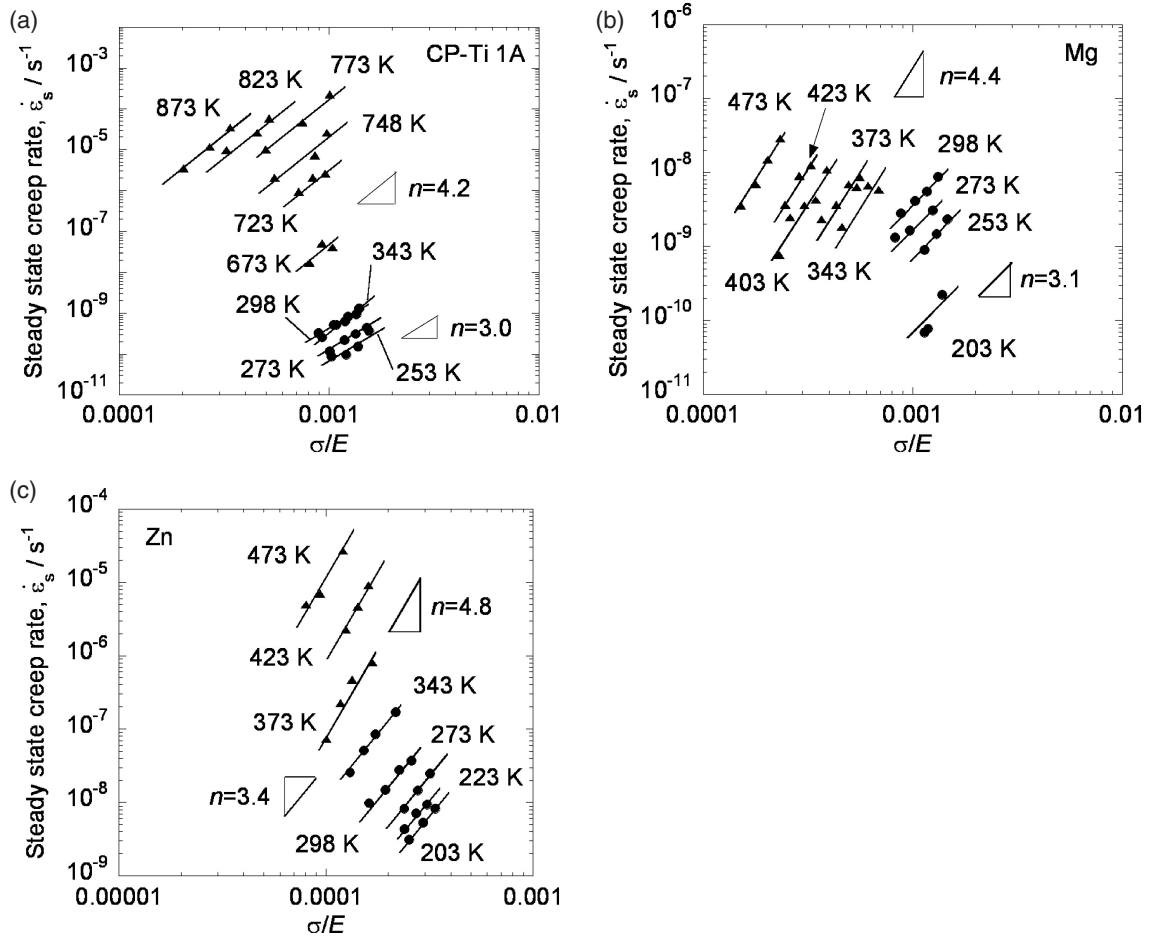
Fig. 5 Double logarithmic plots of the modulus-compensated applied stress and the extrapolated steady state creep rate for (a) CP-Ti 1A, (b) Mg and (c) Zn with $d = 100\,\mu m$. Stress exponents are about 3.0 for all tested metals in the ambient-temperature creep region. Higher-temperature regions corresponded to the low-temperature creep region with dislocation-core diffusion.
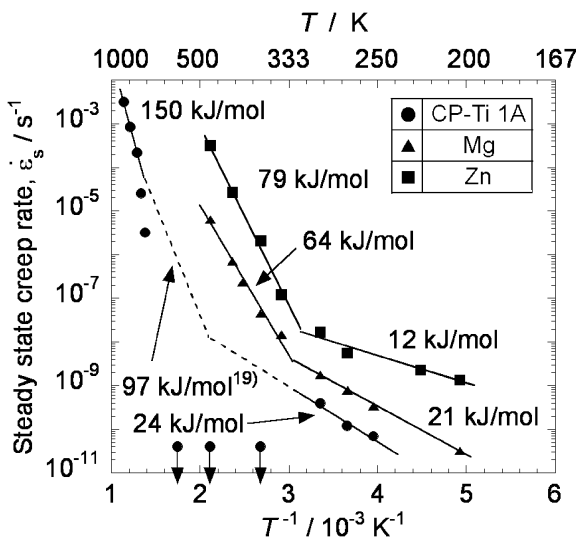
Fig. 6 Arrhenius plots of CP-Ti 1A at $\sigma/E = 0.001$, Mg at $\sigma/E = 0.0008$, and Zn with $d = 100\,\mu m$ at $\sigma/E = 0.0002$. The higher-temperature regions for Mg and Zn correspond to low-temperature dislocation creep with dislocation-core diffusion. For CP-Ti, because of the strain aging effect, the low-temperature dislocation creep region was not observed. The region with $Q = 150\,kJ/mol$ corresponds to high-temperature dislocation creep region with lattice diffusion. The lower-temperature region corresponds to the ambient-temperature creep region with an apparent activation energy of about 20 kJ/mol.
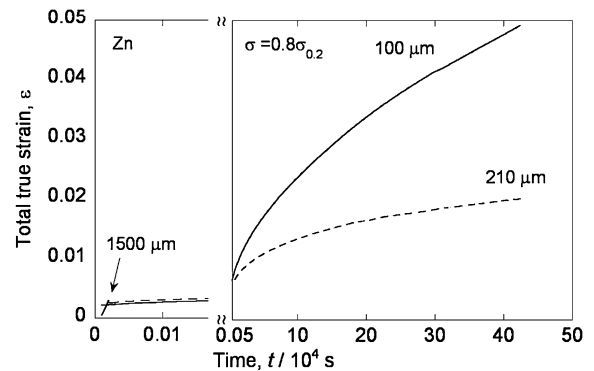
Fig. 7 Grain-size dependence of ambient-temperature creep of Zn under $0.8\sigma_{0.2}$, which corresponds to 32, 19 and 4.8 MPa for specimens with $d = 100$, 210, and 1500 μm, respectively. Increasing grain size decreases the creep strain. In addition, brittle fracture occurred immediately after loading with the largest grain size.

4. Discussion

Ambient-temperature creep was observed in all three pure h.c.p. metals in spite of their different crystallographic c/a ratios. Summarizing the experimental results obtained in this
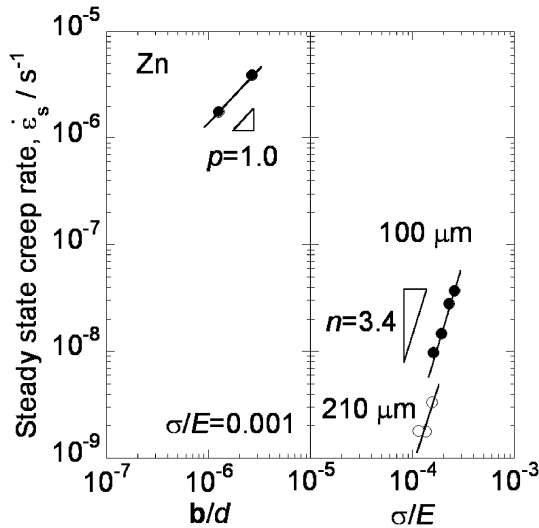
Fig. 8 Double logarithmic plot of the Burgers-vector-compensated grain size and the extrapolated steady-state creep rate (left) and the modulus-compensated applied stress and the extrapolated steady-state creep rate (right) for specimens with $d = 100$ and $210\,\mu m$ of Zn. The figure shows that the $\dot{\varepsilon}_s$ of coarse-grained specimens decreases by one order of magnitude compared with fine-grained specimens, which indicates a grain-size exponent of 1.0.

Fig. 9 Total true strain-time plot of CP-Ti 1A with an initial stress of $160\,MPa$ ($0.92\sigma_{0.2}$). The elastic-after-effect was observed after eliminating the stress completely, but the total true strain did not become zero.

work, we can identify a constitutive relation for ambient temperature creep in the form of the modified Dorn equation:[27]

$$\dot{\varepsilon}_s = AD_0 \exp(-Q/RT)\frac{Gb}{kT}\left(\frac{\sigma}{E}\right)^n\left(\frac{b}{d}\right)^p, \qquad (3)$$

where A is a dimensionless constant, D_0 is a frequency factor, R is the gas constant, and k is Boltzmann's constant. Ambient-temperature creep is characterized using values of $Q \approx 20\,kJ/mol$, $n = 3.0$ and $p = 1.0$, a unique feature among creep mechanisms such as Nabarro-Herring[28,29] Coble,[30] Harper-Dorn[31] and the dislocation climb process.[31]

There are a few papers[33–36] dealing with creep deformation of around ambient temperature. For Al, Luthy et al.[33] claimed that the n value increases with decreasing temperature. However, their data were obtained with larger stresses in the power-law breakdown region, and their data might not represent the creep behavior in Al at low temperatures well. For steels, transient creep was proposed at ambient temperature.[34,35] The testing periods in these studies were too short (maximum: 1200 s) to allow for recognition and analysis of the steady state creep phenomenon. Compare to these studies in Al and steels, the present study observed and analyzed the steady state creep behavior.

Anelastic effect was analyzed in Fig. 9, which shows a total true strain-time plot of CP-Ti 1A following a complete stress drop from an initial stress of 160 MPa ($0.92\sigma_{0.2}$) to zero MPa at total true strain of 0.0075. An elastic-after-effect of strain of about 0.0001 in 15×10^4 s is observed. This implies that dislocations piled up at grain boundaries are caused by a back stress. In the case of Ti-6Al alloy, Neeraj et al.[13] observed no backflow. Although high Peierls stress inhibits the elastic-after-effect in the solid solution strengthening alloy, the effect appears in the pure metal; the two materials showed ambient-temperature creep.
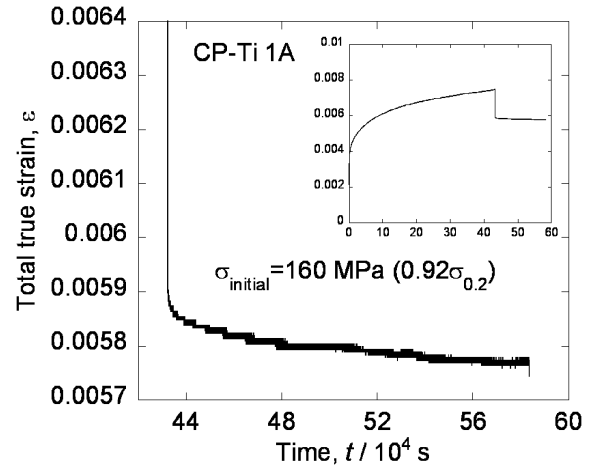
Abnormally low Q values of ambient-temperature creep, about $20\,kJ/mol$, might not activate conventional diffusion accommodated processes. Low Q values of about $25\,kJ/mol$ were observed in creep of Mg-Sc alloys and WE43 at 423–473 K.[36] Koike et al.[37] also reported an low Q value of about $15\,kJ/mol$ in tensile deformation of AZ31 at around room temperature. He claimed that the mechanism is slip-induced grain boundary sliding (GBS),[38–40] which is activated by grain boundary dislocations dissociated by lattice dislocations.

The grain boundary functions as a barrier against dislocation motion, as shown in Fig. 8. Since conventional dislocation creeps at higher temperatures do not depend on the grain-size, this could become a clue in investigations of grain boundary phenomena to reveal the ambient-temperature creep mechanism, which is now underway.

5. Conclusions

Typical pure h.c.p. metals, i.e. CP-Ti, Mg, and Zn, were examined with creep tests at temperatures between 203 K and 873 K, and Arrhenius plots were obtained. These experimental results lead to the following conclusions about ambient-temperature creep.
(1) Ambient-temperature creep appeares below 0.3–0.4 T_m for the tested h.c.p. metals.
(2) The stress exponents of pure h.c.p. metals are 3.0.
(3) The apparent activation energy is evaluated as about $20\,kJ/mol$.
(4) A grain-size exponent of 1.0 is obtained.
(5) A constitutive relation for ambient-temperature creep is obtained as eq. (3).

Acknowledgment

REFERENCES

1) E. Sato, S. Sawai, K. Uesugi, T. Takami, K. Furukawa, M. Kamada and M. Kondo: Mater. Sci. Forum **551–552** (2007) 43–48.
2) T. Yamada, K. Kawabata, E. Sato, K. Kuribayashi and I. Jimbo: Mater. Sci. Eng. A **387–389** (2004) 719–722.
3) H. Adenstedt: Metal Prog. **56** (1949) 658–660.
4) W. R. Kiessel and M. J. Sinnott: Trans. AIME **197** (1953) 331–338.
5) D. R. Luster, W. W. Wentz and D. W. Kaufman: Mater. Methods **37** (1953) 100–103.
6) A. J. Hatch, J. M. Partridge and Broadwell RG: J. Mater. **2** (1967) 111–119.
7) T. F. Kiefer and F. R. Schwartzberg: *NASA-CR-92418* (1967).
8) A. W. Thompson and B. C. Odegard: Metall. Trans. A **4** (1973) 899–908.
9) W. H. Reiman: J. Mater. **6** (1971) 926–940.
10) B. C. Odegard and A. W. Thompson: Metall. Trans. A **5** (1974) 1207–1213.
11) M. A. Imam and C. M. Gilmore: Metall. Trans. A **10** (1979) 419–425.
12) S. Suri, G. B. Viswanathan, T. Neeraj, D. H. Hou and M. J. Mills: Acta Mater. **47** (1999) 1019–1034.
13) T. Neeraj, D. H. Hou, G. S. Daehn and M. J. Mills: Acta Mater. **48** (2000) 1225–1238.
14) T. Neeraj and M. J. Mills: Mater. Sci. Eng. A **319–321** (2001) 415–419.
15) M. F. Savage, J. Tatalovich and M. J. Mills: Phil. Mag. **84** (2004) 1127–1154.
16) T. Neeraj, M. F. Savage, J. Tatalovich, L. Kovaric, R. W. Hayes and M. J. Mills: Phil. Mag. **85** (2005) 279–295.
17) D. Deka, D. S. Joseph, S. Ghosh and M. J. Mills: Metall. Mater. Trans. **37A** (2006) 1371–1388.
18) E. Sato, T. Yamada, H. Tanaka and I. Jimbo: Mater. Trans. **47** (2006) 1121–1126.
19) H. J. Frost and M. F. Ashby: *Deformation mechanism maps*, (Pergamon Press, Oxford, 1982) pp. 43–52.
20) H. Tanaka, T. Yamada, E. Sato and I. Jimbo: Scr. Mater. **54** (2006) 121–124.
21) T. Matsunaga, T. Kameyama, K. Takahashi and E. Sato: Mater. Trans. Submitted.
22) Q. Chen and B. Sundman: Acta Mater. **49** (2001) 947–961.
23) F. Garofalo: *Fundamentals of creep and creep-rupture in metals*, (MacMillan, New York, 1963) sec. 2. 1.
24) J. C. M. Li: Acta Metall. **11** (1963) 1269–1270.
25) N. S. Akulov: Acta Metall. **12** (1964) 1195–1196.
26) R. Boyer, G. Weish and E. W. Collings: *Materials Properties Handbook: Titanium Alloys*: (ASM International, Ohio, 1994) 233–236.
27) T. G. Langdon and F. A. Mohamed: J. Mater. Sci. **13** (1978) 1282–1290.
28) F. R. N. Nabarro: Report of a Conference on Strength of Solid, (The Physical Society, London, 1948) pp. 75–90.
29) C. Herring: J. Appl. Phys. **21** (1950) 437–445.
30) R. L. Coble: J. Appl. Phys. **34** (1963) 1679–1682.
31) J. G. Harper and J. E. Dorn: Acta Metall. **5** (1957) 654–665.
32) J. G. Harper, L. A. Shepard and J. E. Dorn: Acta Metall. **6** (1958) 509–518.
33) H. Luthy, A. K. Miller and O. D. Sherby: Acta Metall. **28** (1980) 169–178.
34) E. Krempl: J. Mech. Phys. Solids **27** (1979) 363–375.
35) A. Oehlert and A. Atrens: Acta Metall. Mater. **42** (1994) 1493–1508.
36) B. L. Mordike: Mater. Sci. Eng. A **324** (2002) 103–112.
37) J. Koike, R. Ohyama, T. Kobayashi, M. Suzuki and K. Maruyama: Mater. Trans. **44** (2003) 445–451.
38) Y. Ishida and M. H. Brown: Acta Metall. **15** (1967) 857–860.
39) R. Z. Valiev and O. A. Kaibyshev: Phys. Status Solidi A **44** (1977) 477–484.
40) P. Mussot, C. Rey and A. Zaoui: Res. Mech. **14** (1985) 69–79.